First retrievals of peroxyacetyl nitrate (PAN) from ground-based FTIR solar spectra recorded at remote sites, comparison with model and satellite data

Emmanuel Mahieu, Emily V. Fischer, Bruno Franco, Mathias Palm, Tyler Wizenberg, Dan Smale, Lieven Clarisse, Cathy Clerbaux, Pierre-François Coheur, James W. Hannigan, et al.

ELEMENTA
Science of the Anthropocene

Mahieu, E, et al. 2021. First retrievals of peroxyacetyl nitrate (PAN) from ground-based FTIR solar spectra recorded at remote sites, comparison with model and satellite data. *Elem Sci Anth*, 9: 1. DOI: https://doi.org/10.1525/elementa.2021.00027

RESEARCH ARTICLE

First retrievals of peroxyacetyl nitrate (PAN) from ground-based FTIR solar spectra recorded at remote sites, comparison with model and satellite data

Emmanuel Mahieu[1,*], Emily V. Fischer[2], Bruno Franco[3], Mathias Palm[4], Tyler Wizenberg[5], Dan Smale[6], Lieven Clarisse[3], Cathy Clerbaux[3,7], Pierre-François Coheur[3], James W. Hannigan[8], Erik Lutsch[5], Justus Notholt[4], Irene Pardo Cantos[1], Maxime Prignon[1], Christian Servais[9], and Kimberly Strong[5]

Peroxyacetyl nitrate (PAN) is the main tropospheric reservoir of NO_x ($NO + NO_2$). Its lifetime can reach several months in the upper cold troposphere. This enables the long-range transport of NO_x radicals, under the form of PAN, far from the regions of emission. The subsequent release of NO_x through the PAN thermal decomposition leads to the efficient formation of tropospheric ozone (O_3), with important consequences for tropospheric oxidative capacity and air quality. The chemical properties of PAN have stimulated the progressive development of remote-sensing products by the satellite community, and recent additions open the prospect for the production of decadal and near-global time series. These products will provide new constraints on the distribution and evolution of this key trace gas in the Earth's atmosphere, but they will also require reliable measurements for validation and characterization of performance. We present an approach that has been developed to retrieve PAN total columns from ground-based high-resolution solar absorption Fourier transform infrared (FTIR) spectra. This strategy is applied to observations recorded at remote FTIR stations of the Network for the Detection of Atmospheric Composition Change (NDACC). The resulting data sets are compared with total column time series derived from IASI (Infrared Atmospheric Sounding Interferometer) satellite observations and to a global chemical transport model. The results are discussed in terms of their overall consistency, mutual agreement, and seasonal cycles. Noticeable is the fact that the FTIR data point to substantial deficiencies in the global model simulation over high latitudes, a poorly sampled region, with an underestimation of the PAN columns during spring, at the peak of the seasonal cycle. Finally, we suggest avenues for development that should make it possible to limit intra- or intersite biases and extend the retrieval of PAN to other NDACC stations that are more affected by water vapor interferences.

Keywords: PAN, Remote-sensing, FTIR technique, NDACC network, Air quality

[1] Institute of Astrophysics and Geophysics, UR SPHERES, Université de Liège, Liège, Belgium

[2] Department of Atmospheric Science, Colorado State University, Fort Collins, CO, USA

[3] Spectroscopy, Quantum Chemistry and Atmospheric Remote Sensing, SQUARES, Université Libre de Bruxelles (ULB), Brussels, Belgium

[4] Institute of Environmental Physics, University of Bremen, Bremen, Germany

[5] Department of Physics, University of Toronto, Toronto, Ontario, Canada

[6] National Institute of Water and Atmospheric Research Ltd., Lauder, New Zealand

[7] LATMOS/IPSL, Sorbonne Université, UVSQ, CNRS, Paris, France

[8] National Center for Atmospheric Research, Boulder, CO, USA

[9] Institute of Astrophysics and Geophysics, STAR Institute, Université de Liège, Liège, Belgium

* Corresponding author:
Email: emmanuel.mahieu@uliege.be

1. Introduction

The number of target species of the ground-based Fourier transform infrared (FTIR) technique is still on the rise. Among the target species relevant for air quality monitoring and forecasting, we find methanol (CH_3OH; e.g., Bader et al., 2014) and ammonia (NH_3; Dammers et al., 2015), in addition to ethane (C_2H_6; e.g., Franco et al., 2016b, Helmig et al., 2016), formaldehyde (HCHO; Franco et al., 2016a), formic acid (HCOOH; e.g., Zander et al., 2010), and carbon monoxide (CO; e.g., Yurganov et al., 2004; Angelbratt et al., 2011). Since (quasi-) simultaneous measurements of all these tracers are available from the broadband FTIR spectra, multispecies studies have also been conducted, showing great potential for studying the impact of biomass burning and wildfire pollution on atmospheric composition in remote locations (e.g., Lutsch et al., 2020). Such FTIR products, available quasi-globally from the Network for the Detection of Atmospheric Composition Change

Table 1. The NDACC FTIR stations involved in the present study and their geographical coordinates. DOI: https://doi.org/10.1525/elementa.2021.00027.t1

Site	Latitude	Longitude	Altitude (m a.s.l.)	Team and Reference
Eureka	80.05° N	86.42° W	610	University of Toronto (Batchelor et al., 2009)
Ny Ålesund	78.92° N	11.93° E	24	University of Bremen (Notholt et al., 1997)
Jungfraujoch	46.55° N	7.98° E	3,580	University of Liège (Zander et al., 2008)
Arrival heights	77.83° S	166.67° E	184	NIWA (Wood et al., 2002)

NDACC = Network for the Detection of Atmospheric Composition Change; FTIR = Fourier transform infrared; NIWA = National Institute of Water and Atmospheric Research Ltd.

(NDACC, http://www.ndacc.org; De Mazière et al., 2018), are also useful for satellite and chemical model validation. Recent investigations include the validation of IASI (Infrared Atmospheric Sounding Interferometer) acetylene (C_2H_2) and hydrogen cyanide (HCN; Duflot et al., 2015), and formic acid (Pommier et al., 2016; Franco et al., 2020), as well as of MOPITT (Measurements of Pollution in the Troposphere) carbon monoxide (Buchholz et al., 2017). New satellite products or sensors require a robust and consistent ground-based FTIR network; for example, such data sets have proved useful for the validation of Sentinel-5 Precursor observations of HCHO product (Vigouroux et al., 2020).

$CH_3COO_2NO_2$, known as peroxyacetyl nitrate (PAN), is another gas subject to sustained investigations by the satellite community, with the aim of producing global remote-sensing measurements for this important NO_x reservoir ($NO_x = NO + NO_2$). PAN is formed when non-methane volatile organic compounds (NMVOCs) oxidation products react with NO_x. Anthropogenic as well as natural emission sources contribute to PAN formation, and these sources include fossil fuel combustion, biomass burning, lightning, and processes responsible for NMVOC emissions (Fischer et al., 2014). The lifetime of PAN against thermal decomposition can reach several months in the cold upper troposphere, and thus, it can be subject to long-range transport and serves as a NO_x source far from the region of primary emission (Tereszchuk et al., 2013; Fischer et al., 2014). Its thermal decomposition in remote areas leads to the efficient formation and redistribution of tropospheric ozone (O_3), with important implications for both tropospheric oxidative capacity and air quality.

Initial results from remote-sensing data have been made available from ACE-FTS (Atmospheric Chemistry Experiment-Fourier Transform Spectrometer) occultation measurements (Tereszchuk et al., 2013), from MIPAS (Michelson Interferometer for Passive Atmospheric Sounding; see, e.g., Glatthor et al., 2007; Moore and Remedios, 2010), and TES (Tropospheric Emission Spectrometer; Payne et al., 2014). Lately, the successful near-global retrieval of PAN has been reported from IASI satellite measurements (Franco et al., 2018). Similarly, important efforts are ongoing for the determination of the global distribution and evolution of PAN from the CrIS (Cross-track Infrared Sounder) instrument, and first data sets have been made available very recently (Bowman, 2021).

To our knowledge, there are no PAN measurements available from ground-based FTIR instruments such as those operated by NDACC. Hence, direct intercomparison of satellite and ground-based column measurements are also lacking, preventing large-scale validation efforts to be undertaken.

In this article, we detail an approach we developed to retrieve PAN from high-resolution ground-based FTIR solar spectra and fill this gap, starting with observations recorded at the high-altitude site of the Jungfraujoch, located in the Swiss Alps. Two different spectral windows of PAN are used, and a complete uncertainty budget is established for each of them as a first objective measure of the retrieval performances. We compare these results with a GEOS-Chem (Goddard Earth Observing System) global chemical transport model (CTM) simulation and with IASI PAN total columns to study the overall agreement between model and observations and characterize the seasonal cycle of PAN at the Jungfraujoch site. We apply this approach to FTIR spectra measured at polar sites in the Northern and Southern hemispheres, in order to check whether the Jungfraujoch retrieval strategy can be usefully implemented at other dry remote sites. We conclude with recommendations for future work.

2. Data sets and tools

2.1. NDACC FTIR stations and retrieval settings

More than 20 high-resolution FTIR spectrometers are currently in regular operation in the framework of NDACC, with broad coverage from Antarctica to the Arctic. Recording high-resolution solar absorption spectra requires clear-sky conditions, leading to temporal sampling typically amounting to a few days per week, year-round, except during the polar night for high-latitude stations. In this article, we make use of observations recorded at dry remote sites, namely Eureka (80° N), Ny Ålesund (78.9° N), Jungfraujoch (46.5° N), and Arrival Heights (77.8° S). More details about the sites are provided in **Table 1**. Two algorithms implementing the Optimal Estimation Method (OEM; Rodgers, 2000) are in use to retrieve geophysical information from ground-based FTIR spectra. In this article, all FTIR teams used SFIT-4 (v0.9.4.4; updated from SFIT-2, see, e.g., Rinsland et al., 1998) to retrieve PAN total columns, but the PROFFIT algorithm (PROFile FIT, e.g., Hase et al., 2004) is also applicable to this purpose. The retrievals are performed using harmonized layering

schemes. Depending on the station, between 41 and 48 layers are defined, with thicknesses increasing progressively from the site altitude up to 120 km, from a few 100 m for the lowermost layers in which water vapor profile is highly structured, up to 14 km thickness for the uppermost layer. It is worth noting that the layering schemes coincide above 5 km altitude, providing a common grid for all NDACC sites. Atmospheric pressure, temperature, and chemical composition are considered homogeneous within these layers. Mean a priori vertical distributions for the target and interfering species were computed from a global multiyear simulation performed for the 1980–2020 time period by the Whole Atmosphere Community Climate Model (WACCM version 4; e.g., Marsh et al., 2013). Midday pressure and temperature profiles are provided by the National Centers for Environmental Prediction (NCEP, Washington, DC; see http://www.ncep.noaa.gov); they are extrapolated above approximately 55 km altitude assuming the WACCM climatology. The spectroscopic parameters adopted in the ground-based retrievals are detailed in Section 3.1. All FTIR instruments are regularly calibrated using HBr and/or N_2O cell measurements and the LINEFIT software (Hase et al., 1999).

2.2. IASI instrument and measurements

IASI is a cross-track Michelson interferometer on the meteorological operation Metop-A, -B, and -C platforms on Sun-synchronous polar orbits, launched in 2006, 2012, and 2018, respectively. It measures the Earth's outgoing radiance in the thermal infrared (IR) spectrum (from 645 to 2,760 cm^{-1} with no spectral gaps) and completes a global coverage twice daily, significantly contributing to the monitoring of Earth's atmospheric composition (Clerbaux et al., 2009).

The PAN vertical abundances are obtained from the IASI observations by applying Version 3 of the Artificial Neural Network for IASI (ANNI). It is a general retrieval framework that already provides global measurements of several volatile organic compounds (VOCs) from IASI spectra (Franco et al., 2018; Franco et al., 2019; Franco et al., 2020). The retrieval procedure consists of two main steps: (1) the gas detection is achieved by the calculation, for each IASI radiance spectrum, of a hyperspectral range index (HRI), a number that reflects the signal strength of a target absorber in a spectral range (Walker et al., 2011). The PAN HRI is calculated in the 760–880 cm^{-1} range (see below); (2) an individual HRI value is converted into PAN total column by an artificial feedforward neural network trained beforehand to map the complex relationships between the PAN HRI, the PAN vertical abundance, and the state of the surface and atmosphere. An uncertainty associated with each retrieved column is also determined. Further explanation on the ANNI v3 retrieval framework and the characterization of the PAN product can be found in Franco et al. (2018) and Clarisse et al. (2019).

The retrieval was applied to each spectrum recorded by IASI/Metop-A (since October 2007) and -B (since March 2013), which represents about 1,300,000 observations per day and per instrument, before prefiltering to scenes with a cloud fraction below 10%. An additional postfilter discards the measurements where the observational sensitivity to PAN is too low to produce a meaningful column. The IASI daily global PAN product employed here uses the European Centre for Medium-range Weather Forecasts Reanalysis Version 5 (ERA5) data set (Hersbach et al., 2020) to describe the state of the surface and atmosphere. The retrieval procedure was applied to both morning and evening IASI satellite overpasses. In the case of PAN, the sensitivity of the evening observations remains satisfactory and consistent with the daytime observations, hence both morning and evening PAN columns are used here.

While the ANNI approach does not produce averaging kernels, an independent analysis using an optimal estimation retrieval approach has shown that the main sensitivity of the IASI measurements to PAN is located between 2 and 10 km altitude and that vertically resolved partial columns are not available. We refer the reader to Franco et al. (2018) for further information on the IASI product for PAN.

2.3. GEOS-Chem model simulation

Our investigations are supported with an O_3-NO_x-VOC-aerosol standard full chemistry GEOS-Chem global CTM simulation (Bey et al., 2001). We used model version 12.0.2 (https://doi.org/10.5281/zenodo.1455215) with MERRA-2 assimilated meteorological fields at $2^\circ \times 2.5^\circ$ (latitude/longitude) horizontal resolution and 72 vertical levels, reaching up to 0.01 hPa (approximately 80 km). This version of GEOS-Chem implements the Harvard Emission Component (HEMCO; Keller et al., 2014) Version 2.1.008 as well as the updates developed and described by Fischer et al. (2014) for the PAN simulation. The adopted inventories include EDGAR v4.3 for fossil fuel emissions, the EMEP and NEI2011 for regional anthropogenic emissions, GFED v4 for fire emissions, MEGAN v2.1 for biogenic emissions, and RETRO for the NMVOC emissions. Following Philip et al. (2016), we set the chemical and transport time steps operators at 20 and 10 min, respectively.

The year 2010 was used to spin up the model and remove the initial conditions. The simulation extends from 2011 through 2014. The model outputs were saved at a 2-h frequency, and a mass conservative regridding tool (see Section 3.1.1 in Bader et al., 2017) has been used to interpolate the simulated profiles from the closest pixel for each of the relevant NDACC stations onto the corresponding SFIT-4 layering scheme. The GEOS-Chem profiles were not smoothed by the FTIR averaging kernels, so that this study will consistently present direct pairwise comparisons involving model, FTIR or IASI data sets at their maximum resolution. Tests showed that smoothed GEOS-Chem columns are not significantly different from the unsmoothed ones, with total column differences at the 1%–2% level. Should a smoothing be applied, the conclusions drawn from the relevant comparisons presented later in the text would remain unchanged.

Table 2. Settings adopted for the retrieval of PAN. DOI: https://doi.org/10.1525/elementa.2021.00027.t2

Spectral Range	Fitted Gases	Spectroscopy	Note
779.9–811.37 (W1)	PAN (p), H_2O (p), O_3 (p), CO_2, CCl_4, HCFC-22, $ClONO_2$, CFC-113	HITRAN 2016 for H_2O, HITRAN 2008 for the other resolved lines, pseudo-lines for PAN, CCl_4, HCFC-22, $ClONO_2$, and CFC-113	The CO_2 Q-branch is fitted with the model of Lamouroux et al. (2010); still, the 790.72–791.47 cm^{-1} region is deweighted to have a signal to noise ratio of 10
1,150.57–1,178.83 (W2)	PAN (p), H_2O (p), O_3 (p), N_2O (p), CFC-12, CH_4, HDO, HFC-23	ATM16 for H_2O, HITRAN 2008 for the other resolved lines, pseudo-lines for PAN, CFC-12, and HFC-23	–

"(p)" means that a profile retrieval is performed for the corresponding gas. Otherwise, a simple scaling of the a priori profile is achieved. All a priori vertical distributions are from WACCM (v4), except for HFC-23 and H_2O (see text). PAN = peroxyacetyl nitrate; WACCM = Whole Atmosphere Community Climate Model; HITRAN = high-resolution transmission molecular absorption database.

3. Application to Jungfraujoch

The Jungfraujoch station is a high-altitude site located on the saddle between the Mönch (4,107 m) and the Jungfrau (4,158 m) Alpine summits, in the Bernese Oberland, Switzerland. The high altitude, combined with the vicinity of the Aletsch Glacier, results in a very dry atmosphere, with only one third of the mean water vapor column left above 3,580 m altitude. Since water vapor is the main interference in the IR spectral region, the spectral scene is of exceptional quality, particularly appropriate to search for new FTIR targets and to develop retrieval approaches which can then be tested at (and tuned for) other sites. In addition, an excellent infrastructure is available for research and, despite its remoteness, the site is accessible year-round by train to researchers and heavy equipment. These were the reasons that led the University of Liège team to install an IR grating instrument as early as in the 1950s to record pioneering atmospheric IR spectra (Zander et al., 2008). High-resolution FTIR observations started in 1984, and since then, the monitoring program has been ongoing without any noticeable interruption, leading to a multidecadal observational data set covering more than 35 years. In the present study, we use a subset of the spectra recorded with the Bruker 120HR spectrometer, which has been in operation at the Jungfraujoch since the early 1990s.

3.1. PAN spectroscopic parameters and spectral retrieval windows

A suite of cross-section measurements by Allen et al. (2005a, 2005b) performed at three atmospheric temperatures (250, 273, and 295 K) provided the laboratory spectra, which still constitutes the basis for the remote sensing of PAN. Several bands are available in the mid-IR, all of which are characterized by broad and unstructured features. As pointed out by Tereszchuk et al. (2013), the most intense feature, centered on 1,740 cm^{-1}, is not useful for the ground-based monitoring of PAN, since it is blinded by strong water vapor lines. Another band near 1,302 cm^{-1} is also located in a blinded spectral range of the ground-based mid-IR spectrum, again by water vapor, but also by methane (CH_4) and nitrous oxide (N_2O) transitions. The two remaining candidate bands are located at 1,163 cm^{-1} (CO stretching) and 794 cm^{-1} (NO_2 bending), in regions populated by numerous interferences by strong water vapor lines, O_3, N_2O, carbon dioxide (CO_2), and other broad absorption features of heavy molecules. In our investigations, we do not use the cross-sections directly. Instead, a pseudo-linelist generated by G. C. Toon (Jet Propulsion Laboratory, California Institute of Technology, Pasadena, CA) is implemented. A description of how the PAN pseudo-line parameters were obtained is available online (https://mark4sun.jpl.nasa.gov/data/spec/Pseudo/Readme.pan).

We use the SFIT-4 (v0.9.4.4) algorithm for the simulation of the PAN candidate spectral windows. The code was updated to allow the simulation and retrieval of trifluoromethane (CHF_3 or HFC-23). Line-by-line spectral parameters from the HITRAN 2008 and 2016 compilations (high-resolution transmission molecular absorption database; Rothman et al., 2009; Gordon et al., 2017) as well as from ATM16 are used (see https://mark4sun.jpl.nasa.gov/toon/atm18/atm18.html; Accessed 25 January 2021), supplemented with pseudo-linelists (available from https://mark4sun.jpl.nasa.gov/pseudo.html; Accessed 25 January 2021) for the interfering unresolved features of, namely, carbon tetrachloride (CCl_4), chlorine nitrate ($ClONO_2$), CFC-12 (CCl_2F_2), HCFC-22 ($CHClF_2$), HFC-23 (CHF_3), and CFC-113 (CCl_2FCClF_2). The solar lines compilation and model described (and maintained) by Hase et al. (2006) are used to fit the nontelluric absorptions present in the selected spectral ranges. The adopted settings are provided in **Table 2**. Panel A of **Figure 1** shows a typical ground-based IR spectrum encompassing the two PAN candidate windows, delimited by the two shaded areas, denoted W1 (794 cm^{-1}) and W2 (1,163 cm^{-1}) on the figure and later in the text. This spectrum was recorded at the NDACC Jungfraujoch station on January 9, 2009, with a maximum optical path difference (OPD) of 82 cm at a solar zenith angle of 79.56°. The additional panels show the weak absorber features (B and C), including PAN, and the strong lines (D and E). Since HFC-23 is not part of the WACCM distribution, we adopted as a priori the ACE-FTS profile of Harrison et al. (2012) for 2007. For water vapor, we implement day-by-day vertical distributions from ERA-Interim, supplemented with WACCM seasonal data for the high-

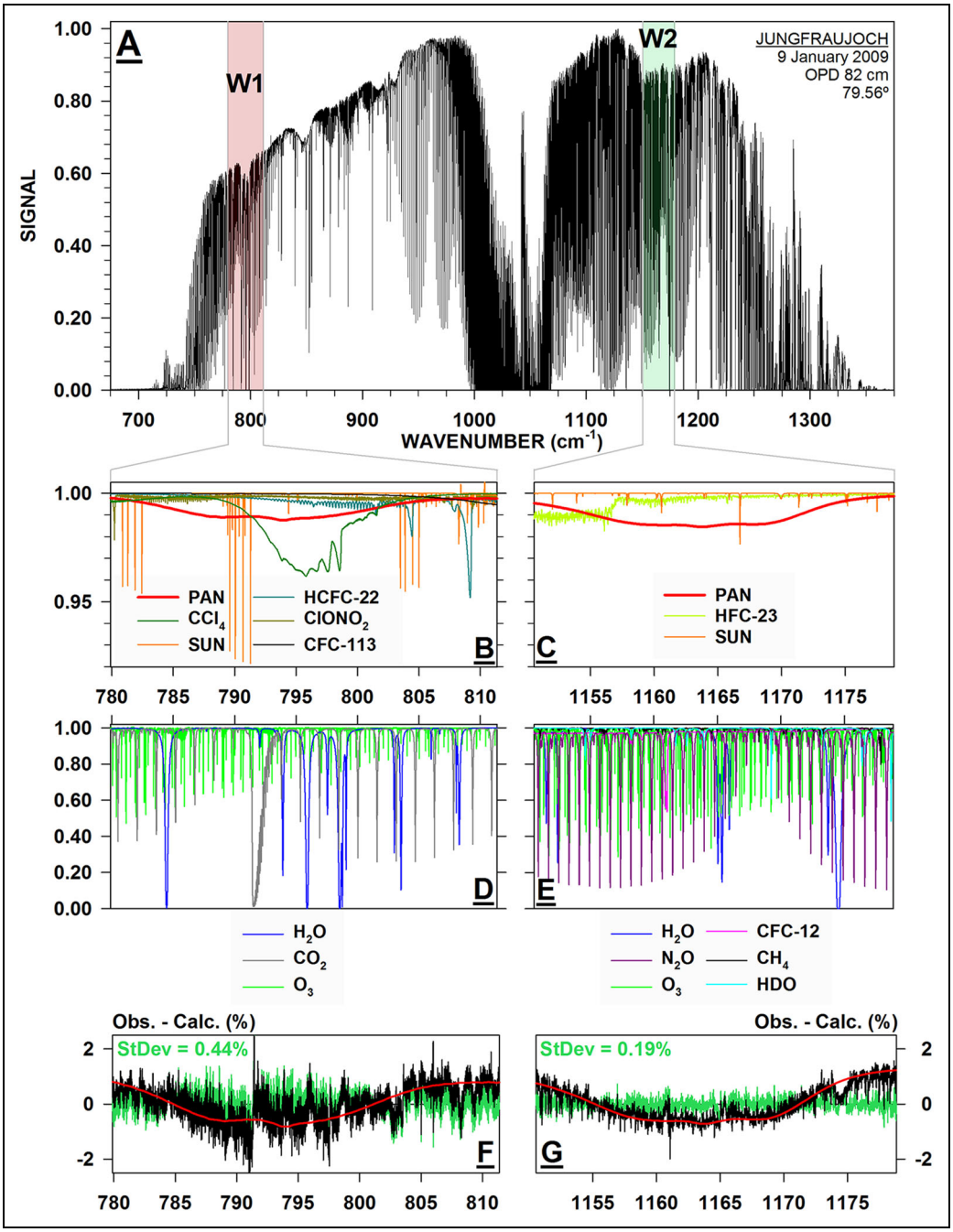

Figure 1. Spectral windows for peroxyacetyl nitrate (PAN). Typical Jungfraujoch spectrum encompassing the two candidate windows for PAN (red- and green-shaded area of Panel A). Panels B and C identify the weak absorbers (among which PAN as the thick red line) in the 794 and 1,163 cm^{-1} windows, respectively. Panels D and E identify the strong absorption lines and features. All simulations have been performed assuming a zenith angle of 79.56° and a maximum optical path difference (OPD) of 82 cm. See the color keys for the identification of the various interferences. Panels F and G show the fitting residuals (observed - calculated; in green) for each spectral range, from the fit to a spectrum recorded on June 23, 2010 (zenith angle of 79.12°, mean total column of 3.7×10^{15} molec. cm^{-2}), when adjusting PAN (green lines for the residuals and red lines for the PAN absorptions) or when zeroing PAN in the simulated spectra (black lines). Note the different *y*-axis ranges throughout the various panels. DOI: https://doi.org/10.1525/elementa.2021.00027.f1

altitude levels. For Jungfraujoch, the PAN a priori column amounts to approximately 2.4×10^{15} molec. cm^{-2}, corresponding to an average tropospheric mixing ratio of 0.24 ppb (see Panel B of **Figure 2**). As is obvious from Panels B and C of **Figure 1**, even for such a low Sun spectrum, the broad and unstructured absorption features of PAN are weak, peaking at 1.3% and 1.5% when assuming the a priori abundance, for W1 and W2, respectively. The main interferences in W1 are shown in Panel D of **Figure 1**; they are due to CO_2, in particular the Q-branch head at 791 cm^{-1}, affected by line-mixing (see Rinsland et al., 2012), some strong water vapor lines, and a suite of ozone

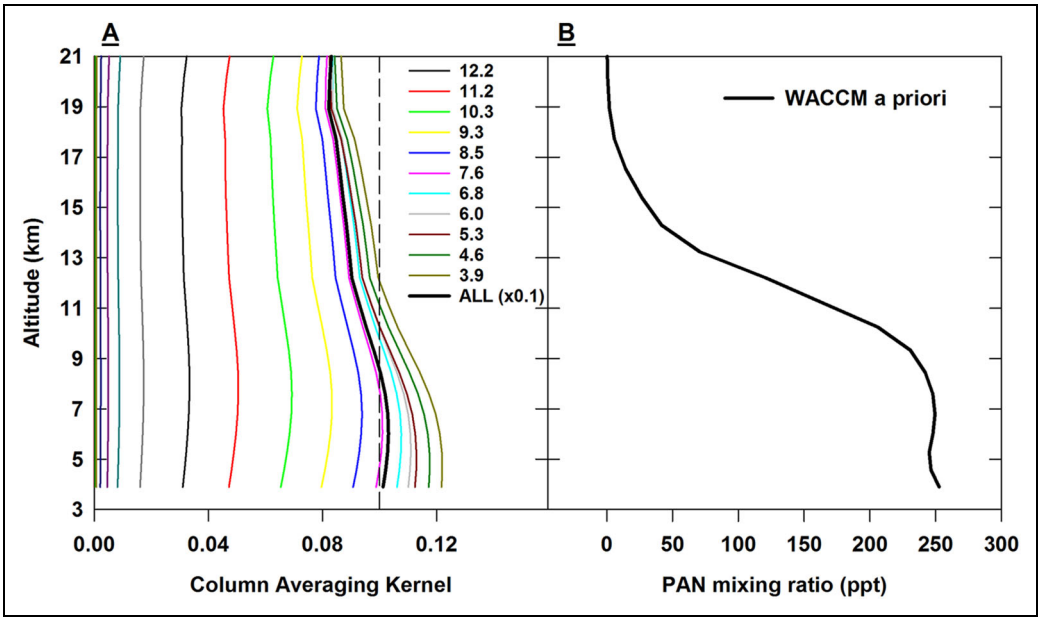

Figure 2. Information content and a priori profile for Jungfraujoch. Typical column averaging kernel for the 11 lowermost layers and the total column (black thick curve), for the 794 cm^{-1} window and the Jungfraujoch station, are reproduced in Panel A. A single piece of information is available, with a mean degree of freedom for signal of 1.02. It essentially characterizes the tropospheric column of peroxyacetyl nitrate (PAN). Information content is similar for the second window; hence it is not shown. Panel B shows the PAN a priori vertical distribution adopted for the Jungfraujoch retrievals. It corresponds to the mean profile derived from a 1980–2020 WACCM simulation. DOI: https://doi.org/10.1525/elementa.2021.00027.f2

lines. The spectral scene is further complicated by the broad CCl_4 feature and some HCFC-22 absorptions. In comparison, the W2 continuum appears less intricate, being mainly influenced by the PAN and the HFC-23 features (see Harrison et al., 2012). There are fewer water vapor lines in W2, but we note that this range encompasses many N_2O and O_3 lines, some significant CFC-12 features as well as some weaker HDO and CH_4 lines (see Panel E of **Figure 1**). The last two panels of **Figure 1** (F for W1 and G for W2) show in green representative fitting residuals obtained when adjusting PAN, for a spectrum recorded on June 23, 2010, at a solar zenith angle of 79.12° and a mean PAN total column of 3.7×10^{15} molec. cm^{-2}. As in previous studies (see, e.g., figure 1 in Franco et al., 2019), we further show in black the residuals obtained when zeroing the PAN contribution in the simulated spectra. The residuals triple for W2 (from 0.19% to 0.57%) while they are degraded by about 50% for W1 (from 0.44% to 0.64%).

3.2. Information content and uncertainty budget

Based on the information presented in the previous section, it is difficult to predetermine which of the W1 or the W2 windows is the most favorable for the retrieval of PAN, even if it is clear from **Figure 1A** that the Jungfraujoch instrumental response provides larger local signal-to-noise ratio for W2. On the one hand and while they indicated that the 794 cm^{-1} window is a possible alternative, Tereszchuk et al. (2013) preferred to use the 1,163 cm^{-1} feature for retrieving PAN from ACE-FTS occultation spectra. On the other hand, Franco et al. (2018) gave preference to the 794 cm^{-1} window for the retrieval of PAN from IASI radiance spectra, as it is less affected by variations in the spectral surface emissivity (e.g., over sandy and rocky soils). We evaluated the respective performance of W1 and W2 by establishing complete uncertainty budgets and analyzing the available information content. **Table 2** provides the retrieval settings adopted for each window. As already indicated, the SFIT-4 algorithm implements the OEM of Rodgers (2000), and the various contributions to the uncertainty budget are computed following the equations and formalism presented in previous papers, for example, in section 2.2 of Zhou et al. (2018).

For both windows, a Tikhonov-type L1 regularization has been adopted. The α parameters have been tuned essentially such as to limit oscillations in the retrieved vertical profiles of PAN. The eventual α values are very close, of 60 and 55 for W1 and W2, respectively. Using a subset of 406 spectra representative of the seasons and observing geometries, we evaluate the typical vertical information. It is limited, with mean degrees of freedom for signals of 1.02 and 1.05, for W1 and W2, respectively. The averaging kernel matrices and corresponding eigenvectors (not shown) are very similar. **Figure 2** shows the mean typical column averaging kernels (Panel A) for W1. For both windows, the retrieval is essentially sensitive to the troposphere, with no vertical resolution available. **Table 3** details the uncertainty budgets established with the subset of 406 spectra for W1 and W2, accounting for the various identified error sources, including both random and systematic components.

Table 3. Mean relative uncertainty affecting the peroxyacetyl nitrate (PAN) total columns retrieved from Window 1 (794 cm^{-1}) or Window 2 (1,163 cm^{-1}), for the random and systematic components. DOI: https://doi.org/10.1525/elementa.2021.00027.t3

Error Type and Source	Relative Uncertainty (%)		Notes
Random components	Window 1	Window 2	
Measurement noise	1.1	0.8	Optimal estimation method (OEM) formalism
Smoothing error	1.0	1.5	OEM formalism
Model parameters	1.4	1.0	OEM formalism
Temperature	6.1	5.3	See text for information on the assumed error patterns
Sun-tracking geometry	0.9	0.9	Assuming 0.1° for solar pointing
Total random in quadrature	**6.5**	**5.7**	
Systematic components			
Retrieval algorithm and forward model	1.0	1.0	Consistent with Duchatelet et al. (2010)
PAN spectroscopy	7.9	7.9	8%—Consistent with Tereszchuk et al. (2013)
Line parameters for main interfering species	2.6	3.7	Considering HITRAN uncertainties for H_2O, CO_2, N_2O, and O_3; consistent with Rinsland et al. (2012) for CCl_4
Temperature	5.8	4.5	See text for information on the assumed error patterns
Instrumental alignment	0.2	0.8	Maximum 10% misalignment
Total systematic in quadrature	**10.2**	**9.9**	
Selection of spectral range limits	20.0	20.0	Comparison with arbitrarily enlarged windows
Total systematic in quadrature	**22.5**	**22.3**	Spectral range limits impact included
Relative standard deviation on the daily means	**7.9**	**4.7**	See text

HITRAN = high-resolution transmission molecular absorption database.

Vertical profiles derived from the WACCM and GEOS-Chem simulations were used to evaluate the atmospheric variability of PAN needed to compute a representative smoothing error. In the troposphere, the diagonal elements of the resulting covariance matrix vary between 50% per km near the surface as well as at the tropopause level, showing lower variability in between, with a minimum value of 35% per km at 6 km. For the extra-diagonal elements of the covariance matrix needed to compute the smoothing error, we assumed an interlayer correlation half-width of 3 km. The contribution of temperature errors on both components of the uncertainty budget were evaluated by assuming random (and systematic) biases of 2 (1) K in the lower- and mid-troposphere, 4 (2) K at the tropopause, 3 (2) K in the lower stratosphere, and 6 (4) K in the upper stratosphere. The retrieved columns for both windows were found essentially insensitive to the choice of the a priori vertical profile, with no significant contribution to the systematic uncertainty budget. Finally, as in previous studies (e.g., Mahieu et al., 2017), solar tracking and instrumental alignment were evaluated to be better than 0.1° and 10%, respectively.

We noticed when setting up and tuning the retrieval strategy that the choice of the windows limits has a non-negligible impact on the derived columns for PAN. In order to appraise it, we performed a few dedicated tests in spectral ranges arbitrarily enlarged by 5–10 cm^{-1}. Changing the windows width essentially led to a systematic bias of the retrieved columns, reaching in some instances up to about 20%, while showing compact correlations between the respective W1 and W2 subsets. Assumptions made regarding the shape of the instrumental response, that is, involving a parabolic instead of a straight line continuum fit, could potentially be another significant source of uncertainty or bias. However, it was not possible to evaluate it as fitting a curvature led to much noisier results, especially in W1, likely because of interplay between the second-order background parameter, the PAN, and the CCl_4 absorptions.

Overall, the total uncertainties reported in **Table 3** are of commensurate magnitudes for W1 and W2. The total systematic errors are on the order of 20%–25% when accounting for the impact of the windows size selection, close to 10% otherwise. They are chiefly influenced by the windows sizes, and then by the uncertainties affecting the spectroscopy of PAN, of the main interferences and the temperature vertical profiles. Regarding the random errors, the situation is slightly more favorable for W2 (5.7%) than for W1 (6.5%), with the largest contribution coming from the uncertainties associated with the

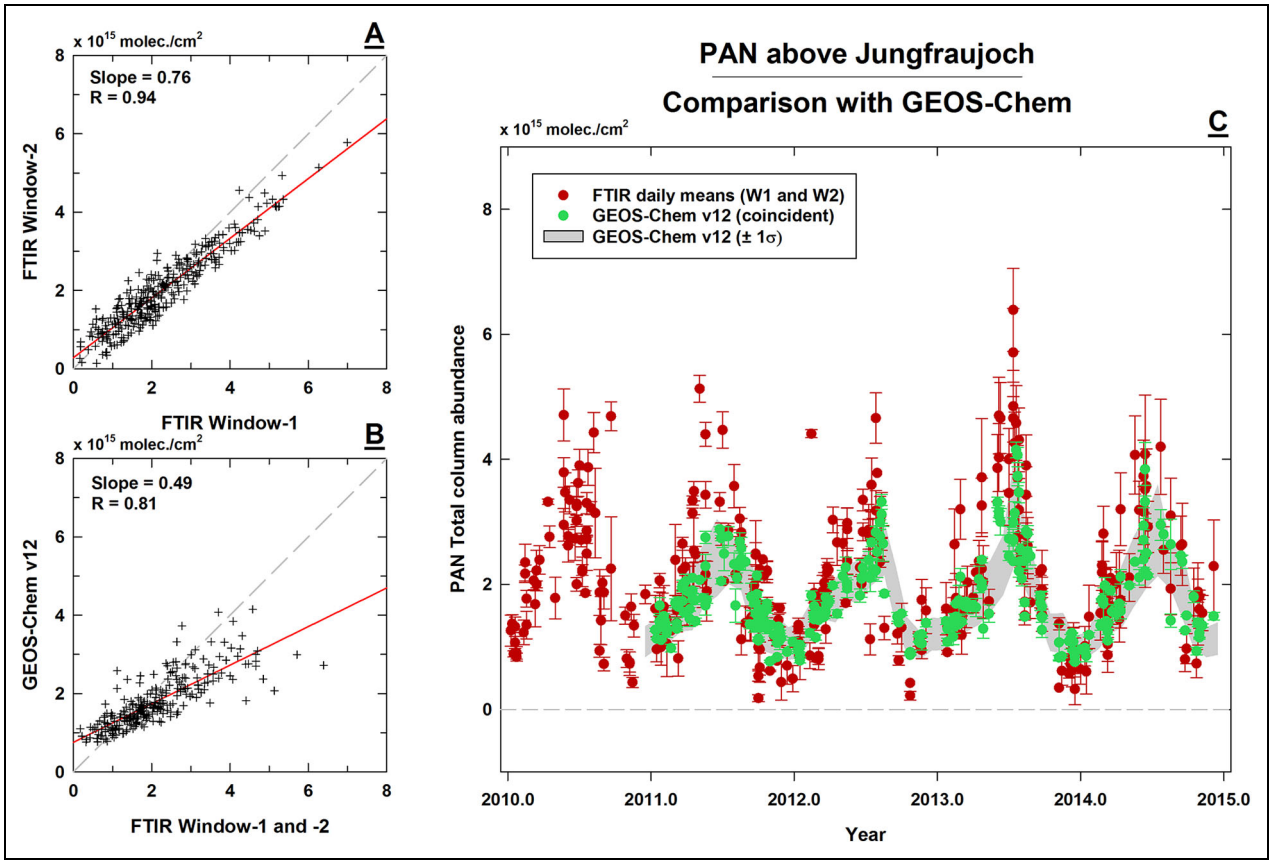

Figure 3. Peroxyacetyl nitrate (PAN) above Jungfraujoch and comparison with Goddard Earth Observing System (GEOS)-Chem. Observed and modeled daily mean total column time series of PAN for the Jungfraujoch station, for 2010–2014. Panel A indicates a compact correlation between the daily averages computed using W1 and W2 data. Panel C shows the PAN time series derived from the Fourier transform infrared (FTIR) observations (W1 and W2 combined; red circles) and the 2° × 2.5° GEOS-Chem simulation (v12.0.2; green circles). In both cases, the error bars correspond to the standard deviation around the daily averages. The gray area represents the range of the monthly mean total columns and associated $\pm 1\sigma$ standard deviation, as derived from the model simulation. Panel B evaluates the consistency between the FTIR (W1 and W2 combined) and GEOS-Chem data. DOI: https://doi.org/10.1525/elementa.2021.00027.f3

temperature profiles. It is worth noting that the mean relative standard deviations on the daily averages—a combined measure of the intraday variability of PAN and of the scatter or noise affecting the retrieved total columns—suggest a more significant advantage for W2 column determinations, with 4.7% for W2 in comparison to 7.9% for W1.

3.3. Observed and modeled PAN for 2010–2014

All ground-based FTIR solar spectra recorded at the Jungfraujoch station between 2010 and 2014 (inclusive) spanning the W1 and W2 spectral ranges have been fitted, using the settings detailed in **Table 2**. This represents a total of 2,751 spectra obtained on 557 days. The two resulting total column subsets were carefully investigated in order to evaluate their mutual consistency. As could be expected given the weak absorption features of PAN shown in **Figure 1** (Panels B and C), our first comparisons indicated that PAN cannot be reliably retrieved from high Sun observations. The strength of the PAN spectral absorptions rapidly drops, peaking at 0.6% for 70°, 0.3% for 50°, and 0.2% for 35°, when assuming its a priori abundance (see Section 3.1). Scatter plots revealed obvious outliers that correspond to spectra recorded with low to medium zenith angles. These outliers can be objectively removed when setting up a threshold for the solar zenith angles equal to 74°, even if reducing the size of our sample by about a half, down to 1443 spectra (352 days). Furthermore, we found that the W2 total columns, unlike the W1 ones, show a linear dependence on the solar zenith angle. Its origin remains unknown, but we decided to correct for it, using the linear relationship and normalizing for 80°. It is worth noting that the HFC-23 total columns retrieved from W2 showed an annual increase close to 1.3 ppt (± 0.3; 2σ) over 2010–2014, commensurate with trends reported by the Advanced Global Atmospheric Gases Experiment in situ network (AGAGE; 0.9 ppt yr^{-1}; see, e.g., tables 1–14 in chapter 1 of WMO, 2014). We conclude that this interference is properly accounted for in our retrievals and that it should not introduce a progressive bias in the PAN total columns deduced from W2.

The consistency between the W1 and W2 FTIR time series for Jungfraujoch is quantitatively evaluated in Panel A of **Figure 3**. This scatter plot includes the 313 pairwise

daily means available after filtering the PAN retrievals for both windows. Fits with negative mixing ratios, with poor residuals, or which did not converge were discarded, reducing the sample sizes by less than 9%. We see a very good correlation, with a *R*-factor of .94 (.86 before correction for the solar zenith angle dependence of the W2 columns), a slope of 0.76 and an intercept of 2.87 $\times$ 10^{14} molec. cm^{-2}. The fractional differences (see equation 2 in Mahieu et al., 2008; using here W2 as "VAL") are characterized by quite a large scatter, influenced mainly by the low total columns measured in winter. The mean (median) value amounts to 9.1% (10.9%; W1 larger than W2). This remains within the combined systematic uncertainties reported in **Table 3**, even when neglecting the impact of the windows sizes on the systematic uncertainty budget. Considering this satisfactory agreement between the W1 and W2 subsets, giving confidence in the retrieved total columns for a difficult target, we combined them in the next steps. Panel C of **Figure 3** shows as red circles the PAN daily mean total columns computed when including all available W1 and W2 measurements for 2010–2014, inclusive. The error bars represent the standard deviations ($\pm 1\sigma$) around the daily averages. We observe a significant seasonal cycle characterized by minimum abundances in winter (November, December, January, and February [NDJF]) and maximum columns in summertime (June, July, and August), about 3 times higher than the background values. Peak-to-peak amplitudes are large, amounting to 123%, with respect to the mean PAN total column for 2010–2014.

We compared these observations with the GEOS-Chem model results presented in Section 2.3, after exclusion of the year 2010, which corresponds to the spin-up of the simulation. The GEOS-Chem columns, available every 2 h, have been combined, and the coincident daily averages are displayed as green circles in the Panel C of **Figure 3**. The corresponding error bars represent the standard deviation around the simulated daily averages, while the gray area shows the $\pm 1\sigma$ standard deviation range around the GEOS-Chem monthly means, including all days year-round. Overall, the modeled time series shows a strong correlation with the observations. The phase of the seasonal modulation is well represented while the amplitude is generally lower, because on the one hand, the low NDJF columns appeared overestimated by the simulation. On the other hand, the peak column values are not captured by the model. The scatter plot shown in Panel B confirms the deviation for the extrema, especially for the high values. A slope close to 0.5 is determined and the *R*-factor of .81 denotes a compact correlation.

3.4. Comparison with IASI-A and IASI-B

In this section, we compare the ground-based FTIR total columns with IASI-A and IASI-B ANNI total columns, for the coincidences available over 2011–2014 and 2013–2014, respectively. The IASI observations have been filtered considering the cloud coverage and were taken within 100 km from the Jungfraujoch. Since we observe a good consistency between IASI-A and IASI-B measurements near the Jungfraujoch for the years 2013–2014, with a correlation coefficient of .82 and a slope that is statistically consistent with the 1:1 line, the IASI data are combined directly, in agreement with previous studies (Franco et al., 2018). Still, the mountainous region surrounding the Jungfraujoch station prevents a direct meaningful comparison between the satellite and the ground-based products. In particular, given the horizontal coverage of the IASI sensors, the mean altitude of the IASI pixels around Jungfraujoch is 1,352 m a.s.l., more than 2 km below the station altitude. Moreover, this mean altitude varies from month to month within a range of only 20 m and is hence representative for all comparisons. Given the significant altitude difference, a pairwise comparison between the IASI and the FTIR total columns shows a steep slope, larger than 1.5 (see Panel A of **Figure 4**). Because there is no vertical information available for the PAN distribution with respect to altitude, it is not possible to compute IASI partial columns above 3.58 km elevation. In order to overcome this obstacle, we use the GEOS-Chem simulation as a transfer standard. From our full chemistry simulation, we further extract a total column time series above 1,352 m altitude, and we compare it to our time series above 3,580 m altitude. A mean (median) column ratio of 1.77 (1.74) is computed (± 0.27, 1σ), and a close correlation is found, with an *R*-factor of .94, a slope of 1.88, and an intercept of -1.57×10^{14} molec. cm^{-2}. We use this linear relationship to scale the IASI columns to the Jungfraujoch station altitude. Panel B of **Figure 4** shows the scatter plot between the scaled satellite columns and the ground-based data, characterized by a slope of 0.8 (± 0.08; 2σ), a correlation coefficient of 0.77, and an intercept of 7.03 (± 1.95; 2σ) $\times$ 10^{14} molec. cm^{-2}. This improved agreement gives credit to the scaling method adopted for the IASI columns. The ground-based and the satellite daily mean time series for coincident days are displayed in Panel C as red and green circles, respectively. This figure confirms a particularly good agreement between the two data sets, which both capture consistent seasonal modulations for this challenging target and a mountainous region, as further confirmed by the gray shaded area that represents the range of the IASI monthly mean total columns and associated $\pm 1\sigma$ standard deviation. Both the IASI and FTIR data sets suggest that the seasonal modulation captured by GEOS-Chem is underestimated in terms of peak-to-peak amplitude, with simulated data for summertime below the observations, especially in the middle of the year. This is confirmed by a three-term Fourier fitting to the three 2011–2014 time series. Similar seasonal cycles are derived for the FTIR and IASI time series, with peak-to-peak amplitudes (with respect to the mean columns) of 123% and 121%, respectively. This is indeed significantly larger than the 93% amplitude derived from the GEOS-Chem simulation. As to the location of the extrema, the peak values are found at the end of June (FTIR), the beginning of July (IASI), and the middle of July (GEOS-Chem); the minima at the end of November (GEOS-Chem), the middle of December (FTIR), and the end of January (IASI).

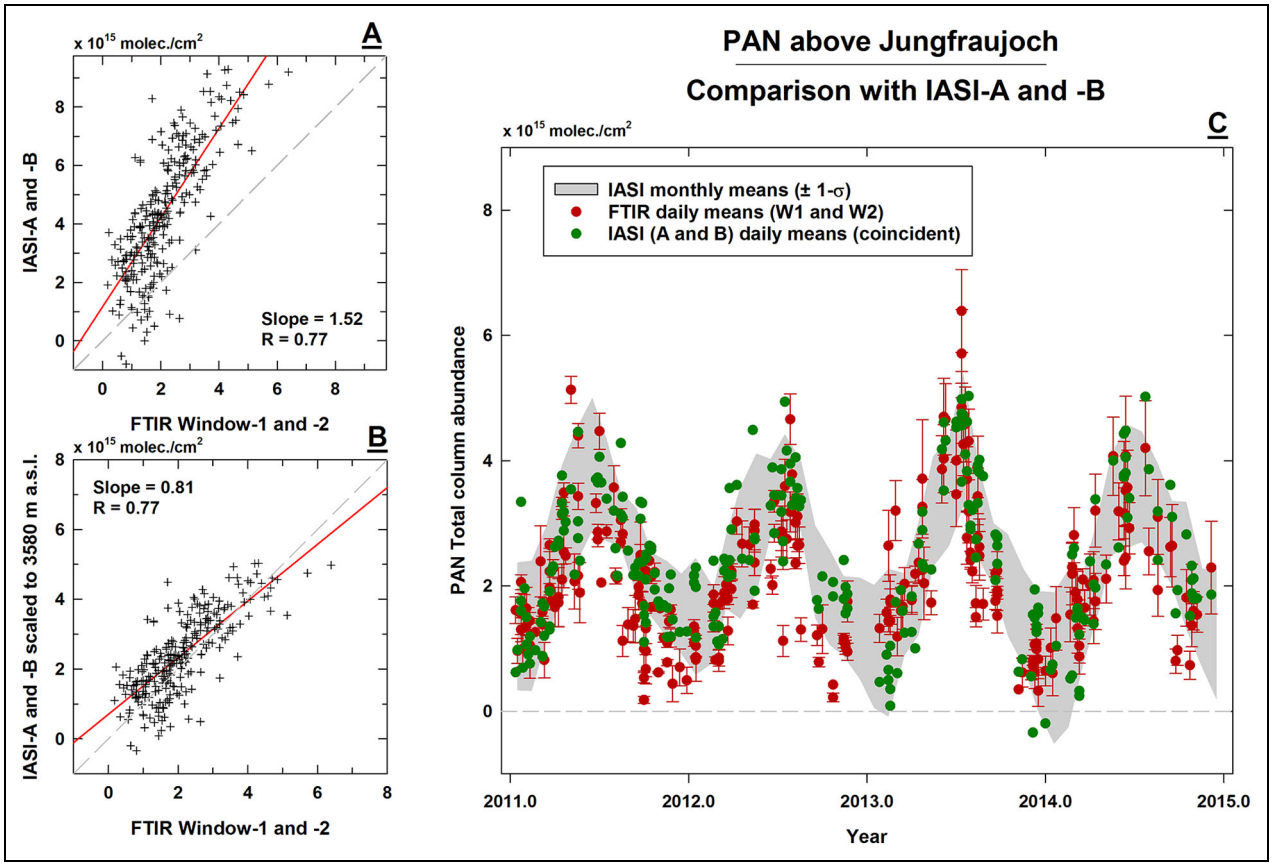

Figure 4. Peroxyacetyl nitrate (PAN) above Jungfraujoch and comparison with infrared atmospheric sounding interferometer (IASI). Comparison between IASI neural network (IASI-A and IASI-B combined) and ground-based Fourier transform infrared (FTIR) total columns (W1 and W2 combined) above the Jungfraujoch station over 4 consecutive years. Panel A (B) shows the scatter plot of the IASI versus FTIR before (after) correction for the Jungfraujoch station altitude (see text). Panel C displays the time series for coincident IASI and FTIR daily means (see color key). The gray area represents the range of the monthly mean total columns and associated $\pm 1\sigma$ standard deviation, as derived from all available IASI observations. DOI: https://doi.org/10.1525/elementa.2021.00027.f4

4. Application to other ground-based FTIR stations

The retrieval approach developed for the Jungfraujoch station has been applied to FTIR spectra recorded at other NDACC sites in order to evaluate its portability. Given the strong interference by water vapor present in the two available spectral regions (see Panels D and E of **Figure 1**), we selected a few polar sites for this first study dealing with ground-based retrievals of PAN, as they are characterized by relatively dry atmospheric conditions. Moreover, it is also interesting to investigate to what extent these cold remote locations are affected by long-range transport and accumulation of this pollutant reservoir. A first common finding is that it was not possible to derive decent results from W2 for any of these additional sites. Inconsistent or even unphysical columns were found. This was somewhat unexpected since this window appears less challenging, with PAN being the sole broad spectral feature affecting the local background (see **Figure 1C**). Also, the achieved signal-to-noise ratios are also supposed to be larger than for W1, minimizing the random noise and uncertainty. We tentatively attribute this poor result to uneven instrumental responses that affect the local background continuum in a way that is not manageable by the SFIT code. The instrumental response is influenced by several factors, including the detector and optical filter responses, the optical elements, and the instrument itself. The atmospheric signal is superimposed on this continuum as illustrated by **Figure 1A**, and a complicated underlying shape different from a slope, a concave, or a convex form cannot be appropriately modeled by SFIT-4, which currently includes at most a second-order polynomial function to deal with the instrumental response and background continuum. Further developments of the code will be needed allowing, for example, to ratio the atmospheric spectra with a laboratory measurement. In the meantime, we present W1 results for three polar sites. Comparisons with GEOS-Chem simulations and IASI observations are included in the next sections whenever available.

4.1. Eureka (80° N)

A subset of the FTIR spectra recorded at the Polar Environment Atmospheric Research Laboratory (PEARL, Eureka station, Ellesmere Island, Nunavut, Canada) has been analyzed, adopting the settings depicted in **Table 2** for W1 (794 cm^{-1}). PAN total columns have been retrieved for the 2010–2013 and 2017–2018 time periods, inclusive. The data showing strong vertical profile

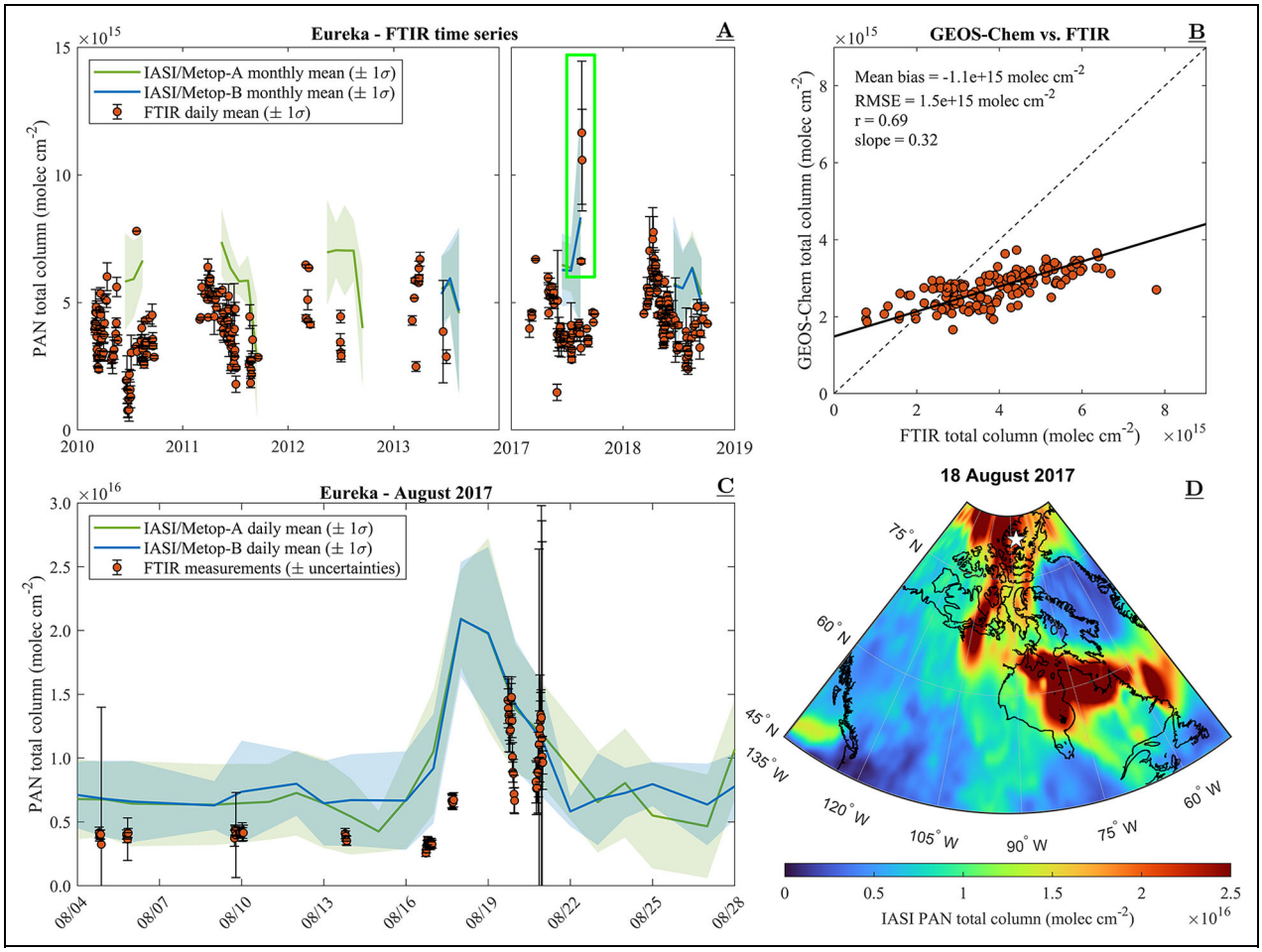

Figure 5. Peroxyacetyl nitrate (PAN) above Eureka. PAN total column measurements for the Eureka station. Panel A displays as red circles and error bars ($\pm 1\sigma$), the Fourier transform infrared (FTIR) total column daily means for the 2010–2013 and 2017–2018 time periods, and the IASI-A and IASI-B monthly mean columns as green and blue solid lines ($\pm 1\sigma$ as shaded areas), respectively. The scatter plot comparing the FTIR and Goddard Earth Observing System (GEOS)-Chem daily mean total columns over 2010–2013 is reproduced in Panel B. Panel C shows the development of the PAN abundance for a few days in August 2017 (corresponding to the green rectangle in Panel A), when a fire plume passed over the Canadian site, as observed by the ground-based and IASI satellite instruments. Panel D reveals the spatial extent of the fire plume at its maximum intensity in terms of PAN abundance above Eureka (identified by the white star), as derived from IASI-A and -B above North America on August 18, 2017. IASI = Infrared Atmospheric Sounding Interferometer. DOI: https://doi.org/10.1525/elementa.2021.00027.f5

oscillations and/or negative mixing ratios were excluded, leaving 1,787 individual measurements spread over 285 different days, from March to September. The corresponding time series is reproduced in Panel A of **Figure 5**. Overall, a mean total column of 4.28×10^{15} molec. cm^{-2} is computed, slightly larger than the a priori columns (approximately 3.8×10^{15} molec. cm^{-2}, mean tropospheric a priori mixing ratio of 0.26 ppb), varying essentially between 1.09 and 7.47×10^{15} molec. cm^{-2} ($\pm 2\sigma$). A seasonal signal is observed, peaking in April, and showing minimum burden in June. The mean peak-to-peak amplitude evaluated with a three-term Fourier series amounts to 56%, with respect to the average total column. It is worth reminding, however, that the solar observations do not provide a complete picture of the seasonal modulation since there is no measurement during the polar night, which extends from late October until late February.

The IASI-A and IASI-B measurements obtained within 100 km from Eureka between 2010 (2013 for IASI-B) and 2018, inclusive, have been averaged. They are shown on **Figure 5A** as continuous lines. The shaded areas display the $\pm 1\sigma$ uncertainty ranges around the means. At polar latitudes, the (quasi-) absence of thermal contrast between the surface and the air layer lying just above reduces significantly the spectral signal recorded by IASI and hampers meaningful retrievals of PAN (and of other weak absorbers in general) during most of the year. Hence, the temporal coverage of the satellite measurements is limited to a few summer months and does not allow investigation of the seasonal cycle. The monthly mean IASI columns vary between 4 and 7×10^{15} molec. cm^{-2}. They show a high bias relative to the ground-based measurements, which likely results from the poor observational conditions or

low thermal contrast frequently encountered by IASI in these polar regions.

A PAN time series has been extracted for Eureka from our v12.0.2 GEOS-Chem full chemistry simulation. A first direct superposition of the model and FTIR data indicates a low bias for GEOS-Chem, with mean fractional differences of 27% ± 31% (1σ). Better agreement is noticeable around the middle of the year, where minimum columns are found for both the model and the observations. For the years 2010–2013, we have 152 days with FTIR measurements available, and the comparison of the GEOS-Chem and FTIR daily means confirms a significant bias for the larger column measurements. Quantitatively, the scatter plot shown in **Figure 5B** indicates a good correlation (*R*-factor of .69), but with a slope of only 0.32. Note that the statistical results are not significantly different when removing the spin-up year (2010). Although in disagreement most of the time as to the magnitude of the PAN total columns, the seasonal cycles revealed by the observations and the model both show a PAN variation throughout the year above Eureka that is quite different from the one above the Jungfraujoch, with its summer maximum.

The FTIR data for 2017 and 2018 confirm the shape of the seasonal cycle and the magnitude of the columns above PEARL. In August 2017, very large PAN columns were retrieved from the ground-based FTIR observations, about 3 times larger than the typical values for that period of the year. Comparisons with IASI-A and IASI-B data have been conducted in order to confirm these outlying columns. Panel C of **Figure 5** portrays as red circles the development of the PAN FTIR columns from August 4 until August 16, daily mean columns close to 4×10^{15} molec. cm^{-2} are observed, before reaching 11.7 and 10.6 $\times 10^{15}$ molec. cm^{-2} on August 19 and 20, respectively. The daily averaged satellite measurements between August 4 and 27 are reproduced as continuous lines on **Figure 5C**, together with the associated ±1σ uncertainty ranges around the daily means (shaded area). The IASI instruments show mean columns close to 7×10^{15} molec. cm^{-2}, with the exception of a few days characterized by peak columns around August 18, before progressively returning to background abundances, as consistently shown by both ensembles. Lutsch et al. (2019) established that a widespread smoke plume was passing at that time above the Eureka site, originating from British Columbia wildfires, the second largest on record in terms of area burned, totaling 1.2 million hectares (BC Wildfire Service, 2017). This episode was further affected by wildfire emissions from the Northwest Territories, leading to simultaneous enhancements in several biomass burning related species, including PAN. The horizontal extent of the PAN plume as captured by IASI on August 18, 2017, is shown in **Figure 5D**. This episode will be further investigated in an upcoming multispecies study.

4.2. Ny Ålesund (79° N)

A multiyear total column time series (2000–2017) of PAN has been retrieved from FTIR solar spectra recorded at Ny Ålesund (Svalbard, 78.9° N), using the W1 spectral range.

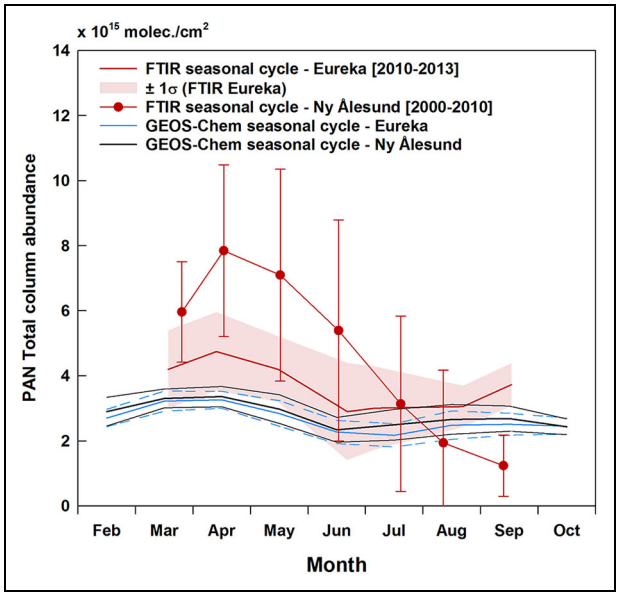

Figure 6. Peroxyacetyl nitrate (PAN) above Ny Ålesund. Comparison between the mean seasonal cycles as derived from the Fourier transform infrared (FTIR) monitoring programs conducted at Ny Ålesund (red circles and error bars, considering all data over 2000–2010) and at Eureka (red curve and area, when including all measurements over 2010–2013). The black curve (and its associated ±1σ envelope delimited by the thin black curves) corresponds to the mean seasonal cycle derived for Ny Ålesund from the Goddard Earth Observing System (GEOS)-Chem simulation over 2011–2014. The corresponding GEOS-Chem results for Eureka are shown in blue (dashed curve for the ±1σ envelope). DOI: https://doi.org/10.1525/elementa.2021.00027.f6

An emerging feature characterizes this data set: The columns obtained for springtime are generally high, reaching levels above 10×10^{15} molec. cm^{-2}, hence significantly larger than for Eureka. This might suggest that important and persistent local sources of pollution could be at play, and/or transport of PAN from Russia, or that there is a systematic high bias in the Ny Ålesund FTIR data. Moreover, the data recorded since 2012 are especially large, following a significant upgrade of the 120HR instrument. The mean seasonal cycle of PAN above Ny Ålesund has therefore been computed considering the data recorded between 2000 and 2010. It is reproduced on **Figure 6** as red circles (error bars correspond to ±1σ). The mean column amounts to 5.8×10^{15} molec. cm^{-2}, that is, about 30% larger than the a priori state (4.4×10^{15} molec. cm^{-2}; mean tropospheric mixing ratio of 0.30 ppb). A clear maximum in terms of column and variability is observed in spring and more specifically in April and May. In the following months, the PAN abundance decreases progressively to reach, in September, levels that are more than 5 times lower. This seasonal cycle is qualitatively consistent with in situ measurements performed at Spitsbergen in the first half of 1994 and reported by Solberg et al. (1997). During these few months, the PAN surface mixing ratios varied on average from 0.18 ppb in February up to

more than 0.30 ppb in March and April. Thereafter, PAN decreased progressively down to about 0.06 ppb in July when the campaign ended. If these surface measurements do not provide a complete picture of the PAN burden, especially for a trace gas that might not be evenly distributed with altitude in the polar troposphere, they do indicate a seasonal modulation in phase with the column observations, suggesting lower concentrations by 30% on average. It should be noted however that the in situ data stand within the $\pm 1\sigma$ range of the PAN concentrations derived from the FTIR time series. As for Eureka, the poor retrieval conditions that prevail at Ny Ålesund do not allow a meaningful comparison between the ground-based FTIR and IASI columns. Lastly, we compare the Ny Ålesund mean seasonal cycle as derived from the FTIR observations with the GEOS-Chem simulation combining the 2011–2014 data (black curves). Although the years considered are noncoincident, we see significant differences for March until May, with both measured and modeled cycles showing maximum columns in spring. The seasonal modulation derived from the Eureka observations over 2010–2013 also confirms this spring maximum, and while the statistical envelopes of the two FTIR sites overlap, the mean total columns are most of the time larger above Ny Ålesund by an amount that can only be partly attributed to the altitude difference of 586 m between both stations.

4.3. Arrival heights (78° S)

The retrieval strategy for PAN was further tested for Arrival Heights, Antarctica (77.8° S). This site is among the most remote FTIR stations, with very little direct influence from anthropogenic emissions and pollution. High-resolution solar spectra for the years 2015–2020 have been systematically fitted, adopting the W1 approach. The fittings proved difficult and either low or negative total columns were derived, leading on average to a near-zero mean. This is likely due to the remoteness of the site, resulting in total columns that are probably below the detection limit of PAN. A mean total column of only 0.43×10^{15} molec. cm^{-2} is computed when considering the GEOS-Chem simulation over the 2011–2014 time frame, to compare with the WACCM a priori total column of 0.57×10^{15} molec. cm^{-2} adopted in the SFIT-4 retrievals. That is more than 6 times smaller than for Eureka or Ny Ålesund.

Under these circumstances and even for low Sun spectra, the PAN absorption would reach a maximum of only 0.1%. The simulated total columns peak in September, but they barely reach values close to 1×10^{15} molec. cm^{-2} while showing extremely low intraday or year-to-year variations.

5. Conclusions and prospects

Using FTIR high-resolution solar absorption spectra recorded at the dry high-altitude station of the Jungfraujoch, we have developed and tuned a retrieval strategy for PAN. The two PAN signatures present in mid-IR "unblinded" spectral ranges are exploited; they result either from CO stretching or NO_2 bending vibrational transitions for a heavy molecule. The associated absorption features are broad, unstructured, and quite weak, forcing the setup and definition of wide windows for the proper retrieval of PAN. In both cases, only limited information content is available, leading to the determination of total columns characterizing essentially the troposphere. W1 and W2 results are found to be very consistent throughout the seasons and time, indicating that PAN is undergoing a significant seasonal modulation, with minimum (maximum) burden in winter (summer). These ground-based FTIR data are successfully compared with a $2° \times 2.5°$ global CTM simulation by GEOS-Chem as well as with nearby measurements by the IASI-A and IASI-B satellite instruments. The good agreement found among all these ensembles gives confidence in the information that can be independently derived from the IR remote-sensing technique for a challenging species.

The Jungfraujoch retrieval strategy was applied to 3 dry and remote NDACC FTIR sites. A first, somewhat unexpected, finding is that the W2 settings failed to convey useful results for PAN at these additional sites. Conversely, the W1 range, while spectrally busier and noisier, allowed the determination of multiyear time series at both the Eureka and Ny Ålesund Arctic sites.

Eureka data show a contrasted seasonal cycle when compared to Jungfraujoch, with largest columns observed in April and minimum columns in June. The seasonal modulation simulated by GEOS-Chem is in good agreement, but with a mean low bias close to 1×10^{15} molec. cm^{-2}. Indeed, the slope of the scatter plot is significantly less than one, while the correlation is found to be quite compact. A test case involving IASI and FTIR measurements demonstrate that both experiments capture very high PAN columns associated with the overpass of a widespread smoke plume from the British Columbia and Northwest Territories intense wildfires which occurred in 2017 and that the magnitude of the satellite and ground-based columns are consistent throughout the period under scrutiny, when accounting for their respective uncertainty bounds.

Application to Ny Ålesund brought additional information. Overall, the observed columns confirm a spring maximum for the Arctic regions, but they generally appeared quite large, especially after a major upgrade of the Bruker 120HR in 2012. This suggests the possible impact of the instrumental response on the derived PAN columns, potentially leading to systematic biases. When restricting to the 2000–2010 data, the derived columns remain larger, on average, than those at Eureka, depicting a seasonal modulation that is primarily characterized by maximum columns in spring and minimum abundances and variability in September.

Finally, the W1 approach has been tested with spectra recorded at Arrival Heights, Antarctica. At this very remote location, the retrievals lead to very low or negative columns, as it is hard to deal with PAN absorption levels that are likely close to the detection limit. Indeed, the GEOS-Chem simulation indicates mean total columns that are about 6 times smaller than for the Arctic sites, corresponding to marginal levels of absorption of about 0.1%, even for low Sun observations.

This study corresponds to a first effort of NDACC investigators to retrieve information for PAN, an important reservoir of pollutants, from ground-based high-resolution spectra. This opens interesting prospects for the production of global multidecadal time series of PAN, since several FTIR stations started regular operation 30 years ago or even before. Among the positive elements, we observe an overall agreement across the sites, with total column time series characterized by significant seasonal modulations and ranges of magnitude consistent with IASI observations and a global GEOS-Chem simulation. Still, we generally observe some underestimation of the PAN burden by the model. Also, we hypothesize that the existing range of FTIR instrumental responses and overall shapes of the background continuum could be responsible for site-to-site bias or for time series discontinuities resulting from instrumental upgrades or replacement. This calls for retrieval software developments before attempts to retrieve PAN from wet sites and network-wide validation efforts can be undertaken. This will be left for future work.

Data accessibility statement

The Fourier transform infrared and infrared atmospheric sounding interferometer data sets as well as the Goddard Earth Observing System (GEOS)-Chem time series presented in this work are available on zenodo.org. The attributed DOI is http://doi.org/10.5281/zenodo.5111613.

The GEOS-Chem model version v12.0.2 can be downloaded from https://doi.org/10.5281/zenodo.1455215. The SFIT-4 core code is publicly available at https://github.com/NCAR/sfit-core-code.

Acknowledgments

We thank the International Foundation High Altitude Research Stations Jungfraujoch and Gornergrat (Bern) for supporting the facilities needed to perform the Fourier transform infrared observations at Jungfraujoch. We thank Canadian Network for the Detection of Atmospheric Change (CANDAC)/Polar Environment Atmospheric Research Laboratory (PEARL)/PAHA PI James Drummond, Canadian Arctic ACE/OSIRIS Validation Campaign PI Kaley Walker, PEARL Site Manager Pierre Fogal, CANDAC Data Manager Yan Tsehtik, the CANDAC operators, and the staff at Environment and Climate Change Canada's Eureka Weather Station for their contributions to data acquisition and for logistical and on-site support. We thank Antarctica New Zealand for providing support for the measurements at Arrival Heights. We thank Olivier Flock (ULiège) for his constant and dedicated support. We are grateful to the many colleagues who contributed to Fourier transform infrared data acquisition, instrument maintenance, and development. We thank Dr G. C. Toon (Jet Propulsion Laboratory, California Institute of Technology, Pasadena, CA) for generating and making available the pseudo-linelists as well as the ATM16 line-by-line compilation, but also for useful discussions about the various factors influencing the retrieval of peroxyacetyl nitrate from ground-based observations.

Funding

The University of Liège (ULiège) team has been primarily supported by the Fonds de la Recherche Scientifique (F.R.S.—FNRS, Brussels, Belgium; grant no. J.0147.18) and by the GAW-CH program of MeteoSwiss (Zürich, Switzerland). E. Mahieu is a senior research associate with the F.R.S.—FNRS. His stay at the Lauder station, New Zealand, was supported by the F.R.S.—FNRS mobility grant n° 35143414. Eureka measurements were made at Polar Environment Atmospheric Research Laboratory by the Canadian Network for the Detection of Atmospheric Change, primarily supported by the Natural Sciences and Engineering Research Council of Canada, the Canadian Space Agency, and Environment and Climate Change Canada. The University of Bremen work has been supported by the German research foundation (DFG) in the project no. 268020496-TRR 172, within the Transregional Collaborative Research Center "ArctiC Amplification: Climate Relevant Atmospheric and SurfaCe Processes, and Feedback Mechanisms (AC)3" in subproject E02. The University of Bremen has further been funded by the German Ministry of Education and Research (BMBF) in the project TROSTRA (01LG1904A) and the by Senate of Bremen. We also thank the AWI Bremerhaven for logistical support at the AWIPEV station in Ny Ålesund and the personnel of the AWIPEV for their work. Measurements at Arrival Heights are core-funded by the National Institute of Water and Atmospheric Research Ltd. (NIWA) through New Zealand's Ministry of Business, Innovation and Employment Strategic Science Investment Fund.

The development of the infrared atmospheric sounding interferometer (IASI) peroxyacetyl nitrate product has been supported by the project Oxygenated Compounds in the Tropical Atmosphere: Variability and Exchanges ([OCTAVE], http://octave.aeronomie.be) of the Belgian Research Action through Interdisciplinary Networks (BRAIN-be) research program (2017–2021; Research project BR/175/A2/OCTAVE) and by the IASI.Flow Prodex arrangement (ESA-BELSPO). L. Clarisse is a research associate supported by the F.R.S.—FNRS. IASI is a joint mission of Eumetsat and the Centre National d'Etudes Spatiales (France). The IASI Level-1C data are distributed in near real time by Eumetsat through the EumetCast system distribution. The National Center for Atmospheric Research is sponsored by the National Science Foundation. J. W. Hannigan is supported under contract by the National Aeronautics and Space Administration (NASA). The MERRA-2 meteorological data products used for driving the Goddard Earth Observing System-Chem simulation have been provided by the Global Modeling and Assimilation Office at NASA Goddard Space Flight Center.

Competing interests

The authors declare that they have no competing interests.

Author contributions

EM has developed the retrieval strategy for peroxyacetyl nitrate (PAN) using Jungfraujoch spectra. The implementation of SFIT-4 at ULiège benefited from the involvement of

MPr. EM ran the Goddard Earth Observing System (GEOS)-Chem simulation needed to support the interpretation of the results. MPa, TW, and DS tested, tuned, and applied the strategy for the Ny Ålesund, Eureka, and Arrival heights sites, respectively. EL assisted with this process for the Eureka site. BF, LC, and PFC are responsible for the Infrared Atmospheric Sounding Interferometer (IASI) PAN product. BF analyzed the IASI data. EM has drafted a first version of the article, which was improved in a first round with contributions from BF, MPa, TW, DS, and IPC. EM prepared all figures, with the exception of **Figure 5**, which was assembled by BF. EVF provided advice on the use of the GEOS-Chem results and expertise on atmospheric PAN. JWH advised on spectral analysis, retrievals, and uncertainties. CS is responsible for the Fourier transform infrared (FTIR) instrumentation maintenance and development at the Jungfraujoch. KS, JN, and DS are the respective PIs of the Eureka, Ny Ålesund, and Arrival Heights FTIR instruments. All coauthors contributed to the editing and final review of this article.

References

Allen, G, Remedios, JJ, Newnham, DA, Smith, KM, Monks, PS. 2005a. Improved mid-infrared cross-sections for peroxyacetyl nitrate (PAN) vapour. *Atmospheric Chemistry and Physics* **5**(1): 47–56. DOI: http://dx.doi.org/10.5194/acp-5-47-2005.

Allen, G, Remedios, JJ, Smith, KM. 2005b. Low temperature mid-infrared cross-sections for peroxyacetyl nitrate (PAN) vapour. *Atmospheric Chemistry and Physics* **5**(11): 3153–3158. DOI: http://dx.doi.org/10.5194/acp-5-3153-2005.

Angelbratt, J, Mellqvist, J, Simpson, D, Jonson, JE, Blumenstock, T, Borsdorff, T, Duchatelet, P, Forster, F, Hase, F, Mahieu, E, Mazière, MD. 2011. Carbon monoxide (CO) and ethane (C_2H_6) trends from ground-based solar FTIR measurements at six European stations, comparison and sensitivity analysis with the EMEP model. *Atmospheric Chemistry and Physics* **11**(17): 9253–9269. DOI: http://dx.doi.org/10.5194/acp-11-9253-2011.

Bader, W, Bovy, B, Conway, S, Strong, K, Smale, D, Turner, AJ, Blumenstock, T, Boone, C, Collaud Coen, M, Coulon, A, Garcia, O. 2017. The recent increase of atmospheric methane from 10 years of ground-based NDACC FTIR observations since 2005. *Atmospheric Chemistry and Physics* **17**(3): 2255–2277. DOI: http://dx.doi.org/10.5194/acp-17-2255-2017.

Bader, W, Stavrakou, T, Muller, J-F, Reimann, S, Boone, CD, Harrison, JJ, Flock, O, Bovy, B, Franco, B, Lejeune, B, Servais, C. 2014. Long-term evolution and seasonal modulation of methanol above Jungfraujoch (46.5° N, 8.0° E): Optimisation of the retrieval strategy, comparison with model simulations and independent observations. *Atmospheric Measurement Techniques* **7**(11): 3861–3872. DOI: http://dx.doi.org/10.5194/amt-7-3861-2014.

Batchelor, RL, Strong, K, Lindenmaier, R, Mittermeier, RL, Fast, H, Drummond, JR, Fogal, PF. 2009. A new Bruker IFS 125HR FTIR spectrometer for the Polar Environment Atmospheric Research Laboratory at Eureka, Nunavut, Canada: Measurements and comparison with the existing Bomem DA8 spectrometer. *Journal of Atmospheric and Oceanic Technology* **26**(7): 1328–1340. DOI: http://dx.doi.org/10.1175/2009JTECHA1215.1.

BC Wildfire Service. 2017. Wildfire season summary—Province of British Columbia. Available at https://www2.gov.bc.ca/gov/content/safety/wildfire-status/about-bcws/wildfire-history/wildfire-season-summary. Accessed 30 January 2019.

Bey, I, Jacob, DJ, Yantosca, RM, Logan, JA, Field, BD, Fiore, AM, Li, Q, Liu, HY, Mickley, LJ, Schultz, MG. 2001. Global modeling of tropospheric chemistry with assimilated meteorology: Model description and evaluation. *Journal of Geophysical Research Atmospheres* **106**(D19): 23073–23095. DOI: http://dx.doi.org/10.1029/2001JD000807.

Bowman, KW. 2021. TROPESS CrIS-SNPP L2 Peroxyacytyl nitrate for forward stream, standard product V1, Greenbelt, MD, USA, Goddard Earth Sciences Data and Information Services Center (GES DISC). Accessed 14 July 2021. DOI: http://dx.doi.org/10.5067/MQITF51HVPNW.

Buchholz, RR, Deeter, MN, Worden, HM, Gille, J, Edwards, DP, Hannigan, JW, Jones, NB, Paton-Walsh, C, Griffith, DWT, Smale, D, Robinson, J. 2017. Validation of MOPITT carbon monoxide using ground-based Fourier transform infrared spectrometer data from NDACC. *Atmospheric Measurement Techniques* **10**(5): 1927–1956. DOI: http://dx.doi.org/10.5194/amt-10-1927-2017.

Clarisse, L, Clerbaux, C, Franco, B, Hadji-Lazaro, J, Whitburn, S, Kopp, AK, Hurtmans, D, Coheur, P-F. 2019. A decadal data set of global atmospheric dust retrieved from IASI satellite measurements. *Journal of Geophysical Research Atmospheres* **124**(3): 1618–1647. DOI: http://dx.doi.org/10.1029/2018JD029701.

Clerbaux, C, Boynard, A, Clarisse, L, George, M, Hadji-Lazaro, J, Herbin, H, Hurtmans, D, Pommier, M, Razavi, A, Turquety, S, Wespes, C. 2009. Monitoring of atmospheric composition using the thermal infrared IASI/MetOp sounder. *Atmospheric Chemistry and Physics* **9**(16): 6041–6054. DOI: http://dx.doi.org/10.5194/acp-9-6041-2009.

Dammers, E, Vigouroux, C, Palm, M, Mahieu, E, Warneke, T, Smale, D, Langerock, B, Franco, B, Van Damme, M, Schaap, M, Notholt, J. 2015. Retrieval of ammonia from ground-based FTIR solar spectra. *Atmospheric Chemistry and Physics* **15**(22): 12789–12803. DOI: http://dx.doi.org/10.5194/acp-15-12789-2015.

De Mazière, M, Thompson, AM, Kurylo, MJ, Wild, JD, Bernhard, G, Blumenstock, T, Braathen, GO, Hannigan, JW, Lambert, JC, Leblanc, T, McGee, TJ. 2018. The Network for the Detection of Atmospheric Composition Change (NDACC): History, status and perspectives. *Atmospheric Chemistry and*

Physics DOI: http://dx.doi.org/10.5194/acp-18-4935-2018.

Duchatelet, P, Demoulin, P, Hase, F, Ruhnke, R, Feng, W, Chipperfield, MP, Bernath, PF, Boone, CD, Walker, KA, Mahieu, E. 2010. Hydrogen fluoride total and partial column time series above the Jungfraujoch from long-term FTIR measurements: Impact of the line-shape model, characterization of the error budget and seasonal cycle, and comparison with satellite and model data. *Journal of Geophysical Research Atmospheres* **115**(D22). DOI: http://dx.doi.org/10.1029/2010JD014677.

Duflot, V, Wespes, C, Clarisse, L, Hurtmans, D, Ngadi, Y, Jones, N, Paton-Walsh, C, Hadji-Lazaro, J, Vigouroux, C, De Mazière, M, Metzger, JM. 2015. Acetylene (C_2H_2) and hydrogen cyanide (HCN) from IASI satellite observations: Global distributions, validation, and comparison with model. *Atmospheric Chemistry and Physics* **15**(18): 10509–10527. DOI: http://dx.doi.org/10.5194/acp-15-10509-2015.

Fischer, EV., Jacob, DJ, Yantosca, RM, Sulprizio, MP, Millet, DB, Mao, J, Paulot, F, Singh, HB, Roiger, A, Ries, L, Talbot, RW. 2014. Atmospheric peroxyacetyl nitrate (PAN): A global budget and source attribution. *Atmospheric Chemistry and Physics* **14**(5): 2679–2698. DOI: http://dx.doi.org/10.5194/acp-14-2679-2014.

Franco, B, Clarisse, L, Stavrakou, T, Müller, J, Van Damme, M, Whitburn, S, Hadji-Lazaro, J, Hurtmans, D, Taraborrelli, D, Clerbaux, C, Coheur, PF. 2018. A general framework for global retrievals of trace gases from IASI: Application to methanol, formic acid, and PAN. *Journal of Geophysical Research Atmospheres* **123**(24). DOI: http://dx.doi.org/10.1029/2018JD029633.

Franco, B, Clarisse, L, Stavrakou, T, Müller, J -F., Pozzer, A, Hadji-Lazaro, J, Hurtmans, D, Clerbaux, C, Coheur, P-F. 2019. Acetone atmospheric distribution retrieved from space. *Geophysical Research Letters* **46**(5): 2884–2893. DOI: http://dx.doi.org/10.1029/2019GL082052.

Franco, B, Clarisse, L, Stavrakou, T, Müller, J-F., Taraborrelli, D, Hadji-Lazaro, J, Hannigan, JW, Hase, F, Hurtmans, D, Jones, N, Lutsch, E. 2020. Spaceborne measurements of formic and acetic acid: A global view of the regional sources. *Geophysical Research Letters* 1–12. DOI: http://dx.doi.org/10.1029/2019gl086239.

Franco, B, Mahieu, E, Emmons, LK, Tzompa-Sosa, ZA, Fischer, EV, Sudo, K, Bovy, B, Conway, S, Griffin, D, Hannigan, JW, Strong, K. 2016a. Evaluating ethane and methane emissions associated with the development of oil and natural gas extraction in North America. *Environmental Research Letters* **11**(4): 044010. DOI: http://dx.doi.org/10.1088/1748-9326/11/4/044010.

Franco, B, Marais, EA, Bovy, B, Bader, W, Lejeune, B, Roland, G, Servais, C, Mahieu, E. 2016b. Diurnal cycle and multi-decadal trend of formaldehyde in the remote atmosphere near 46° N. *Atmospheric Chemistry and Physics* **16**(6): 4171–4189. DOI: http://dx.doi.org/10.5194/acp-16-4171-2016.

Glatthor, N, von Clarmann, T, Fischer, H, Funke, B, Grabowski, U, Höpfner, M, Kellmann, S, Kiefer, M, Linden, A, Milz, M, Steck, T. 2007. Global peroxyacetyl nitrate (PAN) retrieval in the upper troposphere from limb emission spectra of the Michelson Interferometer for Passive Atmospheric Sounding (MIPAS). *Atmospheric Chemistry and Physics* **7**(11): 2775–2787. DOI: http://dx.doi.org/10.5194/acp-7-2775-2007.

Gordon, IE, Rothman, LS, Hill, C, Kochanov, RV, Tan, Y, Bernath, PF, Birk, M, Boudon, V, Campargue, A, Chance, KV, Drouin, BJ. 2017. The HITRAN2016 molecular spectroscopic database. *Journal of Quantitative Spectroscopy and Radiative Transfer* **203**: 3–69. DOI: http://dx.doi.org/10.1016/j.jqsrt.2017.06.038.

Harrison, JJ, Boone, CD, Brown, AT, Allen, NDC, Toon, GC, Bernath, PF. 2012. First remote sensing observations of trifluoromethane (HFC-23) in the upper troposphere and lower stratosphere. *Journal of Geophysical Research Atmospheres* **117**(D5). DOI: http://dx.doi.org/10.1029/2011JD016423.

Hase, F, Blumenstock, T, Paton-Walsh, C. 1999. Analysis of the instrumental line shape of high-resolution Fourier transform IR spectrometers with gas cell measurements and new retrieval software. *Applied Optics* **38**(15): 3417–3422. OSA. DOI: http://dx.doi.org/10.1364/AO.38.003417.

Hase, F, Demoulin, P, Sauval, AJ, Toon, GC, Bernath, PF, Goldman, A, Hannigan, JW, Rinsland, CP. 2006. An empirical line-by-line model for the infrared solar transmittance spectrum from 700 to 5000 cm^{-1}. *Journal of Quantitative Spectroscopy and Radiative Transfer* **102**(3): 450–463. DOI: http://dx.doi.org/10.1016/j.jqsrt.2006.02.026.

Hase, F, Hannigan, JW, Coffey, MT, Goldman, A, Höpfner, M, Jones, NB, Rinsland, CP, Wood, SW. 2004. Intercomparison of retrieval codes used for the analysis of high-resolution, ground-based FTIR measurements. *Journal of Quantitative Spectroscopy and Radiative Transfer* **87**(1): 25–52. DOI: http://dx.doi.org/10.1016/j.jqsrt.2003.12.008.

Helmig, D, Rossabi, S, Hueber, J, Tans, P, Montzka, SA, Masarie, K, Thoning, K, Plass-Duelmer, C, Claude, A, Carpenter, LJ, Lewis, AC. 2016. Reversal of global atmospheric ethane and propane trends largely due to US oil and natural gas production. *Nature Geoscience* **9**(7): 490–495. DOI: http://dx.doi.org/10.1038/ngeo2721.

Hersbach, H, Bell, B, Berrisford, P, Hirahara, S, Horányi, A, Muñoz-Sabater, J, Nicolas, J, Peubey, C, Radu, R, Schepers, D, Simmons, A. 2020. The ERA5 global reanalysis. *Quarterly Journal of the Royal Meteorological Society* **146**(730): 1999–2049. DOI: http://dx.doi.org/10.1002/qj.3803.

Keller, CA, Long, MS, Yantosca, RM, Da Silva, AM, Pawson, S, Jacob, DJ. 2014. HEMCO v1.0: A versatile, ESMF-compliant component for calculating

emissions in atmospheric models. *Geoscientific Model Development* **7**(4): 1409–1417. DOI: http://dx.doi.org/10.5194/gmd-7-1409-2014.

Lamouroux, J, Tran, H, Laraia, AL, Gamache, RR, Rothman, LS, Gordon, IE, Hartmann, J-M. 2010. Updated database plus software for line-mixing in CO_2 infrared spectra and their test using laboratory spectra in the 1.5–2.3μm region. *Journal of Quantitative Spectroscopy and Radiative Transfer* **111**(15): 2321–2331. DOI: http://dx.doi.org/10.1016/j.jqsrt.2010.03.006.

Lutsch, E, Strong, K, Jones, DBA, Blumenstock, T, Conway, S, Fisher, JA, Hannigan, JW, Hase, F, Kasai, Y, Mahieu, E, Makarova, M. 2020. Detection and attribution of wildfire pollution in the Arctic and northern midlatitudes using a network of Fourier-transform infrared spectrometers and GEOS-Chem. *Atmospheric Chemistry and Physics* **20**(21): 12813–12851. DOI: http://dx.doi.org/10.5194/acp-20-12813-2020.

Lutsch, E, Strong, K, Jones, DBA, Ortega, I, Hannigan, JW, Dammers, E, Shephard, MW, Morris, E, Murphy, K, Evans, MJ, Parrington, M. 2019. Unprecedented atmospheric ammonia concentrations detected in the high arctic from the 2017 Canadian Wildfires. *Journal of Geophysical Research Atmospheres*, in press. DOI: http://dx.doi.org/10.1029/2019JD030419.

Mahieu, E, Duchatelet, P, Demoulin, P, Walker, KA, Dupuy, E, Froidevaux, L, Randall, C, Catoire, V, Strong, K, Boone, CD, Bernath, PF. 2008. Validation of ACE-FTS v2.2 measurements of HCl, HF, CCl_3F and CCl_2F_2 using space-, balloon- and ground-based instrument observations. *Atmospheric Chemistry and Physics* **8**(20): 6199–6221. DOI: http://dx.doi.org/10.5194/acp-8-6199-2008.

Mahieu, E, Lejeune, B, Bovy, B, Servais, C, Toon, GC, Bernath, PF, Boone, CD, Walker, KA, Reimann, S, Vollmer, MK, O'Doherty, S. 2017. Retrieval of HCFC-142b (CH_3CClF_2) from ground-based high-resolution infrared solar spectra: Atmospheric increase since 1989 and comparison with surface and satellite measurements. *Journal of Quantitative Spectroscopy and Radiative Transfer* **186**: 96–105. Elsevier. DOI: http://dx.doi.org/10.1016/j.jqsrt.2016.03.017.

Marsh, DR, Mills, MJ, Kinnison, DE, Lamarque, J-F, Calvo, N, Polvani, LM. 2013. Climate change from 1850 to 2005 Simulated in CESM1(WACCM). *Journal of Climate* **26**(19): 7372–7391. DOI: http://dx.doi.org/10.1175/JCLI-D-12-00558.1.

Moore, DP, Remedios, JJ. 2010. Seasonality of peroxyacetyl nitrate (PAN) in the upper troposphere and lower stratosphere using the MIPAS-E instrument. *Atmospheric Chemistry and Physics* **10**(13): 6117–6128. DOI: http://dx.doi.org/10.5194/acp-10-6117-2010.

Notholt, J, Toon, G, Stordal, F, Solberg, S, Schmidbauer, N, Becker, E, Meier, A, Sen, B. 1997. Seasonal variations of atmospheric trace gases in the high Arctic at 79° N. *Journal of Geophysical Research Atmospheres* **102**(D11): 12855–12861. DOI: http://dx.doi.org/10.1029/97JD00337.

Payne, VH, Alvarado, MJ, Cady-Pereira, KE, Worden, JR, Kulawik, SS, Fischer, E V. 2014. Satellite observations of peroxyacetyl nitrate from the Aura tropospheric emission spectrometer. *Atmospheric Measurement Techniques* **7**(11): 3737–3749. DOI: http://dx.doi.org/10.5194/amt-7-3737-2014.

Philip, S, Martin, R V, Keller, CA. 2016. Sensitivity of chemistry-transport model simulations to the duration of chemical and transport operators: A case study with GEOS-Chem v10-01. *Geoscientific Model Development* **9**(5): 1683–1695. DOI: http://dx.doi.org/10.5194/gmd-9-1683-2016.

Pommier, M, Clerbaux, C, Coheur, P-F, Mahieu, E, Müller, J-F, Paton-Walsh, C, Stavrakou, T, Vigouroux, C. 2016. HCOOH distributions from IASI for 2008–2014: Comparison with ground-based FTIR measurements and a global chemistry-transport model. *Atmospheric Chemistry and Physics* **16**(14): 8963–8981. DOI: http://dx.doi.org/10.5194/acp-16-8963-2016.

Rinsland, CP, Jones, NB, Connor, BJ, Logan, JA, Pougatchev, NS, Goldman, A, Murcray, FJ, Stephen, TM, Pine, AS, Zander, R, Mahieu, E. 1998. Northern and southern hemisphere ground-based infrared spectroscopic measurements of tropospheric carbon monoxide and ethane. *Journal of Geophysical Research* **103**(D21): 28197. DOI: http://dx.doi.org/10.1029/98JD02515.

Rinsland, CP, Mahieu, E, Demoulin, P, Zander, R, Servais, C, Hartmann, J-M. 2012. Decrease of the carbon tetrachloride (CCl_4) loading above Jungfraujoch, based on high resolution infrared solar spectra recorded between 1999 and 2011. *Journal of Quantitative Spectroscopy and Radiative Transfer* **113**(11): 1322–1329. Elsevier. DOI: http://dx.doi.org/10.1016/j.jqsrt.2012.02.016.

Rodgers, CD. 2000. *Inverse methods for atmospheric sounding*. World Scientific. (Series on Atmospheric, Oceanic and Planetary Physics; vol. 2). DOI: http://dx.doi.org/10.1142/3171.

Rothman, LS, Gordon, IE, Barbe, A, Benner, DC, Bernath, PF, Birk, M, Boudon, V, Brown, LR, Campargue, A, Champion, J-P, Chance, K. 2009. The HITRAN 2008 molecular spectroscopic database. *Journal of Quantitative Spectroscopy and Radiative Transfer* **110**(9–10): 533–572. DOI: http://dx.doi.org/10.1016/j.jqsrt.2009.02.013.

Solberg, S, Krognes, T, Stordal, F, Hov Beine, HJ, Jaffe, DA, Clemitshaw, KC, Penkett, SA. 1997. Reactive nitrogen compounds at Spitsbergen in the Norwegian Arctic. *Journal of Atmospheric Chemistry* **28**(1–3): 209–225. DOI: http://dx.doi.org/10.1023/A:1005883323285.

Tereszchuk, KA, Moore, DP, Harrison, JJ, Boone, CD, Park, M, Remedios, JJ, Randel, WJ, Bernath, PF. 2013. Observations of peroxyacetyl nitrate (PAN) in the upper troposphere by the Atmospheric Chemistry Experiment-Fourier Transform Spectrometer

(ACE-FTS). *Atmospheric Chemistry and Physics* **13**(11): 5601–5613. DOI: http://dx.doi.org/10.5194/acp-13-5601-2013.

Vigouroux, C, Langerock, B, Bauer Aquino, CA, Blumenstock, T, Cheng, Z, De Mazière, M, De Smedt, I, Grutter, M, Hannigan, JW, Jones, N, Kivi, R. 2020. TROPOMI-Sentinel-5 Precursor formaldehyde validation using an extensive network of ground-based Fourier-transform infrared stations. *Atmospheric Measurement Techniques* **13**(7): 3751–3767. DOI: http://dx.doi.org/10.5194/amt-13-3751-2020.

Walker, JC, Dudhia, A, Carboni, E. 2011. An effective method for the detection of trace species demonstrated using the MetOp infrared atmospheric sounding interferometer. *Atmospheric Measurement Techniques* **4**(8): 1567–1580. DOI: http://dx.doi.org/10.5194/amt-4-1567-2011.

Wood, SW, Bodeker, GE, Boyd, IS, Jones, NB, Connor, BJ, Johnston, P V, Matthews, WA, Nichol, SE, Murcray, FJ, Nakajima, H, Sasano, Y. 2002. Validation of version 5.20 ILAS HNO3, CH_4, N_2O, O_3, and NO_2 using ground-based measurements at Arrival Heights and Kiruna. *Journal of Geophysical Research Atmospheres* **107**(D24): ILS 5-1-ILS 5-11. DOI: http://dx.doi.org/10.1029/2001JD000581.

World Meteorological Organization. 2014. *Scientific assessment of ozone depletion: 2014, World meteorological organization, global ozone research and monitoring project*—Report No. 55, 416 p., Geneva, Switzerland.

Yurganov, LN, Blumenstock, T, Grechko, EI, Hase, F, Hyer, EJ, Kasischke, ES, Koike, M, Kondo, Y, Kramer, I, Leung, F-Y, Mahieu, E. 2004. A quantitative assessment of the 1998 carbon monoxide emission anomaly in the Northern Hemisphere based on total column and surface concentration measurements. *Journal of Geophysical Research Atmospheres* **109**(D15). DOI: http://dx.doi.org/10.1029/2004JD004559.

Zander, R, Duchatelet, P, Mahieu, E, Demoulin, P, Roland, G, Servais, C, Auwera, JV., Perrin, A, Rinsland, CP, Crutzen, PJ. 2010. Formic acid above the Jungfraujoch during 1985–2007: Observed variability, seasonality, but no long-term background evolution. *Atmospheric Chemistry and Physics* **10**(20): 10047–10065. DOI: http://dx.doi.org/10.5194/acp-10-10047-2010.

Zander, R, Mahieu, E, Demoulin, P, Duchatelet, P, Roland, G, Servais, C, De Mazière, M, Reimann, S, Rinsland, CP. 2008. Our changing atmosphere: Evidence based on long-term infrared solar observations at the Jungfraujoch since 1950. *Science of The Total Environment* **391**(2–3): 184–195. DOI: http://dx.doi.org/10.1016/j.scitotenv.2007.10.018.

Zhou, M, Langerock, B, Vigouroux, C, Wang, P, Hermans, C, Stiller, G, Walker, KA, Dutton, G, Mahieu, E, De Mazière, M. 2018. Ground-based FTIR retrievals of SF_6 on Reunion Island. *Atmospheric Measurement Techniques* **11**(2): 651–662. DOI: http://dx.doi.org/10.5194/amt-11-651-2018.

How to cite this article: Mahieu, E, Fischer, EV, Franco, B, Palm, M, Wizenberg, T, Smale, D, Clarisse, L, Clerbaux, C, Coheur, P-F, Hannigan, JW, Lutsch, E, Notholt, J, Pardo Cantos, I, Prignon, M, Servais, C, Strong, K. 2021. First retrievals of peroxyacetyl nitrate (PAN) from ground-based FTIR solar spectra recorded at remote sites, comparison with model and satellite data. *Elementa: Science of the Anthropocene* 9(1). DOI: https://doi.org/10.1525/elementa.2021.00027

Domain Editor-in-Chief: Detlev Helmig, Boulder AIR LLC, Boulder, CO, USA

Associate Editor: Paul Palmer, School of GeoSciences, The University of Edinburgh, Edinburgh, United Kingdom

Knowledge Domain: Atmospheric Science

Published: September 28, 2021 **Accepted:** August 6, 2021 **Submitted:** April 3, 2021

ELEMENTA Science of the Anthropocene

Elem Sci Anth is a peer-reviewed open access journal published by University of California Press.

OPEN ACCESS